The Astrophysical Journal, 934:15 (5pp), 2022 July 20 https://doi.org/10.3847/1538-4357/ac795e

Observing Supernova Neutrino Light Curves with Super-Kamiokande. III. Extraction of Mass and Radius of Neutron Stars from Synthetic Data

Yudai Suwa[1,2], Akira Harada[3], Masayuki Harada[4], Yusuke Koshio[4,5], Masamitsu Mori[1], Fumi Nakanishi[4], Ken'ichiro Nakazato[6], Kohsuke Sumiyoshi[7], and Roger A. Wendell[5,8]
[1] Department of Earth Science and Astronomy, The University of Tokyo, Tokyo 153-8902, Japan; suwa@yukawa.kyoto-u.ac.jp
[2] Center for Gravitational Physics and Quantum Information, Yukawa Institute for Theoretical Physics, Kyoto University, Kyoto 606-8502, Japan
[3] Interdisciplinary Theoretical and Mathematical Sciences Program (iTHEMS), RIKEN, Wako, Saitama 351-0198, Japan
[4] Department of Physics, Okayama University, Okayama 700-8530, Japan
[5] Kavli Institute for the Physics and Mathematics of the Universe (Kavli IPMU, WPI), Todai Institutes for Advanced Study, The University of Tokyo, Kashiwa 277-8583, Japan
[6] Faculty of Arts and Science, Kyushu University, Fukuoka 819-0395, Japan
[7] National Institute of Technology, Numazu College of Technology, Numazu 410-8501, Japan
[8] Department of Physics, Kyoto University, Kyoto 606-8502, Japan
Received 2022 April 18; revised 2022 June 8; accepted 2022 June 14; published 2022 July 21

Abstract

Neutrinos are guaranteed to be observable from the next Galactic supernova (SN). Optical light and gravitational waves are also observable, but may be difficult to observe if the location of the SN in the Galaxy or the details of the explosion are unsuitable. The key to observing the next SN is to first use neutrinos to understand various physical quantities and then link them to other signals. In this paper, we present Monte Carlo sampling calculations of neutrino events from Galactic SN explosions observed with Super-Kamiokande. The analytical solution of neutrino emission, which represents the long-term evolution of the neutrino light curve from SNe, is used as a theoretical template. It gives the event rate and event spectrum through inverse beta decay interactions with explicit model parameter dependence. Parameter estimation is performed on these simulated sample data by fitting least squares using the analytical solution. The results show that the mass, radius, and total energy of a remnant neutron star produced by an SN can be determined with an accuracy of $\sim 0.1\ M_{\odot}$, $\sim$1 km, and $\sim 10^{51}$ erg, respectively, for a Galactic SN at 8 kpc.

Unified Astronomy Thesaurus concepts: Supernova neutrinos (1666); Neutrino astronomy (1100); Neutrino telescopes (1100); Core-collapse supernovae (304); Neutron stars (1108)

1. Introduction

The next Galactic supernova (SN) would provide a plethora of neutrinos that will likely be detected by a number of neutrino facilities such as Super-Kamiokande (Scholberg 2012; Horiuchi & Kneller 2018). While optical radiation and gravitational waves are also expected from SN bursts, they may be difficult to observe if circumstances are unfavorable. For instance, any optical signals would be absorbed by the interstellar medium if the SN occurs near the Galactic anticenter.[9] In addition, the expected amplitude of any gravitational wave from an SN is both highly uncertain and strongly model dependent, so it is unclear whether they can be detected for all types of explosions. Neutrinos, on the other hand, are strongly penetrating and known to be produced in abundance, making them a guaranteed signal that can be used to study the explosion and its mechanism. Therefore, it will be critical to connect this neutrino signal with other messengers from the next SN to extract the most information from the event (Nakamura et al. 2016; Warren et al. 2020). In particular, understanding neutrinos at late times (>1 s after the onset of explosion) is essential, since the physics surrounding this timescale has much smaller theoretical uncertainties than that of earlier times.

Recently, late-time SN neutrino emission has received much attention. Nakazato et al. (2013), for example, conducted systematic protoneutron star (PNS) cooling simulations starting from the iron core's collapse up to 20 s after the explosion. Furthermore, Suwa et al. (2019), conducted simulations with the same method, but simulated beyond 100 s and investigated a data analysis method called backward time analysis. The work of Roberts et al. (2012) presented similar simulations, while also accounting for convection inside the PNS (see also Li et al. 2021; Pascal et al. 2022). In addition to the PNS cooling simulations described above, there are also hydrodynamics simulations (Fischer et al. 2010; Hüdepohl et al. 2010; Mirizzi et al. 2016; Mori et al. 2021). However, these simulations are spherically symmetric (i.e., 1D) for the long-term evolution ($\gtrsim$10 s) and require special initial conditions or artificial treatment to produce an explosion (but see Suwa 2014, in which a 2D simulation was used for a self-consistent explosion followed by a 1D simulation of the evolution up to 67 s). More recent computational and technical advances allow for relatively long ($\gtrsim$1 s) yet still systematic simulations in 2D or 3D (Nakamura et al. 2019; Vartanyan et al. 2019; Bollig et al. 2021; Burrows & Vartanyan 2021; Nagakura et al. 2021). With these simulations multidimensional effects such as convection, standing-accretion shock instabilities, and lepton-number emission self-sustained asymmetries are naturally included in the neutrino signal. However, computational

[9] Note that Adams et al. (2013) showed that almost all SNe can be found, depending on the Galactic dust model.

constraints nonetheless continue to limit the extension of these studies to later times.

Neutrino observations are sensitive to the physical quantities that characterize the central compact object left behind by an SN explosion. For example, the gravitational binding energy of the SN1987A event was estimated using its neutrino signal (Sato & Suzuki 1987; Burrows 1988). Since that binding energy, $E_{\rm b}$, is related to both the mass, M, and the radius, R, of the PNS through $E_{\rm b}\sim M^2R^{-1}$, it is difficult to make independent estimates of all three parameters. However, independent estimates of M and R would provide a deep understanding of nuclear physics through the nuclear equation of state (see, e.g., Fischer et al. 2014). Therefore, we should aim to use neutrinos from the next Galactic SN to determine M and R independently. Since it is unknown whether neutrinos alone can achieve this goal, in this paper we analyze simulated neutrino spectra to understand the limits of estimating these parameters.

This paper is arranged as follows. Section 2 describes how Monte Carlo calculations are used to create mock samples and Section 3 describes how the generated mock samples are analyzed. Section 4 describes the error evaluation from the data analysis method, and Section 5 summarizes the main results.

2. Mock Sampling

In this work, we use the solution for the neutrino light curve derived in Suwa et al. (2021), in which the time evolution of the event rate and positron average energy are given by analytic functions of time. The parameter dependence on the mass and radius of the neutron star are also explicitly presented.

The event rate is given by

$$\mathcal{R} = 720\ {\rm s}^{-1}\left(\frac{M_{\rm det}}{32.5\ {\rm kton}}\right)\left(\frac{D}{10\ {\rm kpc}}\right)^{-2} \times\left(\frac{M_{\rm PNS}}{1.4\,M_\odot}\right)^{15/2}\left(\frac{R_{\rm PNS}}{10\ {\rm km}}\right)^{-8}\left(\frac{g\beta}{3}\right)^{5} \times\left(\frac{t+t_0}{100\ {\rm s}}\right)^{-15/2}, \quad (1)$$

where $M_{\rm det}$ is the detector mass and 32.5 kton corresponds to the entire inner detector volume of Super-Kamiokande (SK),[10] D is the distance between the SN and Earth, $M_{\rm PNS}$ is the PNS mass, $R_{\rm PNS}$ is the PNS radius,[11] g is the density correction factor, and β is the opacity boosting factor from coherent scattering (see Suwa et al. 2021, for details). The timescale t_0 is given by

$$t_0 = 210\ {\rm s}\left(\frac{M_{\rm PNS}}{1.4\,M_\odot}\right)^{6/5}\left(\frac{R_{\rm PNS}}{10\ {\rm km}}\right)^{-6/5} \times\left(\frac{g\beta}{3}\right)^{4/5}\left(\frac{E_{\rm tot}}{10^{52}\ {\rm erg}}\right)^{-1/5}, \quad (2)$$

[10] In this study, we employ the full 32.5 kton volume of the SK inner detector. This is because at least for a Galactic SN the timescale of data analysis is short and we can avoid significant contamination from backgrounds (Super-Kamiokande Collaboration et al. 2022). For a more detailed discussion, see Suwa et al. (2019).

[11] This corresponds to the radius after PNS contraction by neutrino cooling.

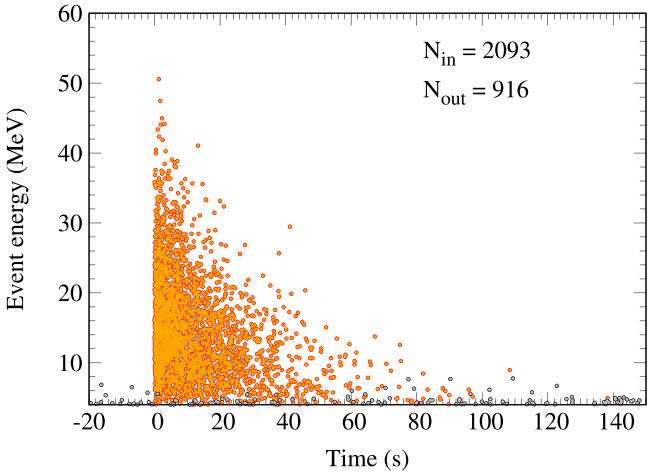

Figure 1. An example scatterplot of positron energy as a function of time for a single simulation. The orange points indicate the signal and the gray points indicate the background. In this particular case, there are 3009 events detected, where 2093 are within the fiducial volume (22.5 kton) and 916 are not therein.

where $E_{\rm tot}$ is the total energy emitted by all flavors of neutrinos. By integrating Equation (1) with Equation (2), the expected total number of events is

$$N = \int_0^\infty \mathcal{R}(t)\,dt = 89\left(\frac{M_{\rm det}}{32.5\ {\rm kton}}\right)\left(\frac{D}{10\ {\rm kpc}}\right)^{-2}\left(\frac{M_{\rm PNS}}{1.4\,M_\odot}\right)^{-3/10} \times\left(\frac{R_{\rm PNS}}{10\ {\rm km}}\right)^{-1/5}\left(\frac{g\beta}{3}\right)^{-1/5}\left(\frac{E_{\rm tot}}{10^{52}\ {\rm erg}}\right)^{13/10}. \quad (3)$$

For the canonical parameters used in this paper ($M_{\rm det}=32.5$ kton, $D=8$ kpc, $M_{\rm PNS}=1.52M_\odot$, $R_{\rm PNS}=11.8$ km, $g\beta=1.6$, and $E_{\rm tot}=10^{53}$ erg), the expectation becomes $N=2970$.

The average energy of created positrons is given by

$$E_{e^+} = 25.3\ {\rm MeV}\left(\frac{M_{\rm PNS}}{1.4\,M_\odot}\right)^{3/2} \times\left(\frac{R_{\rm PNS}}{10\ {\rm km}}\right)^{-2}\left(\frac{g\beta}{3}\right)\left(\frac{t+t_0}{100\ {\rm s}}\right)^{-3/2}. \quad (4)$$

For the energy distribution, we employ the Fermi–Dirac distribution function for neutrinos, which allows us to calculate the distribution of the positron as given in the Appendix. Note that the analysis shown in this paper uses only the average energy of Equation (4) and the spectrum information is not included. As the results of Nakazato et al. (2022) indicate that measurements of the average positron energy are largely insensitive to the details of the neutrino energy distribution, this choice is not expected to impact the results of the analysis below. Note also that the above estimates are based on the simple expression for the cross section of the inverse beta decay. More precise expressions are given in Vogel & Beacom (1999) and Strumia & Vissani (2003), which we used for our numerical estimates in Nakazato et al. (2022).

Using these equations, we simulate 100 Monte Carlo realizations of an SN with our canonical parameters. Figure 1 shows an example. We also plot the expected detector background modeled using Mori (2021) and the Super-

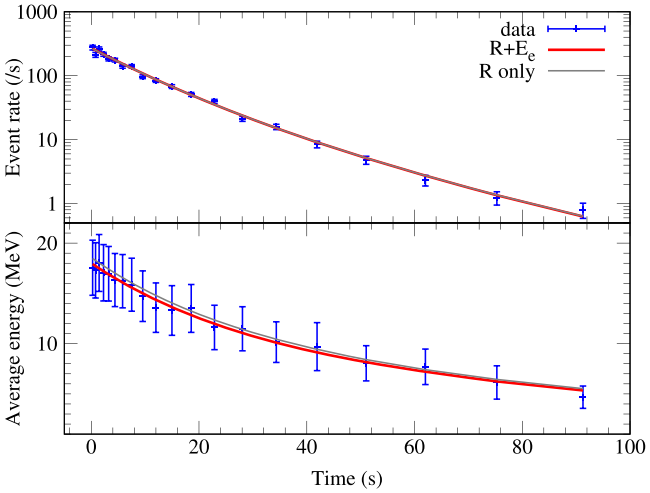

Figure 2. Time evolution of the event rate (top) and average energy (bottom) from the simulation in Figure 1. The error bar on the event rate is the Poisson statistical error, while that for the average energy the error is taken from the standard deviation of the energies observed in that bin. Data are shown by blue points with error bars, the best-fit models using the event rate alone are shown by the gray line, and the red line shows the fit using both the rate and average energy.

Kamiokande Collaboration et al. (2022). This background is not otherwise used in the following analysis, but will be discussed in the forthcoming paper. Note that the neutrino detection lasts for about 100 s, far beyond the timescale of current simulations using detailed treatments of neutrino-radiation hydrodynamics. Accordingly, the analytic neutrino light curve is useful for filling this timescale gap.

3. Data Analysis

In this paper, we use a least-squares fit to estimate the SN parameters from the simulated data. The χ^2 is given by

$$\chi^2 = \sum_{i=1}^{N} \frac{(O_i - X_i)^2}{\sigma_i^2}, \tag{5}$$

where O_i, X_i, and σ_i are the observed value, the expected value, and the variance, respectively, with the time index i. For the event rate ($X = \mathcal{R}$), we use $\sigma_i^2 = \mathcal{R}_i^2/N_i$, where N_i is the event number in the ith bin. For the average energy ($X = E_{e^+}$), we use $\sigma_i^2 = (0.05E_{e^+})^2$ following Nakazato et al. (2022), in which the statistical error of the average energy is shown as several percent levels. We calculate the joint probability density function (PDF) for the measured parameters as

$$\mathcal{P}(M_{\rm PNS}, R_{\rm PNS}, E_{\rm tot}) \propto e^{-\chi^2(M_{\rm PNS}, R_{\rm PNS}, E_{\rm tot})/2}. \tag{6}$$

Figure 2 shows the time evolution of the event rate and average energy of the model shown in Figure 1. The time bins are calculated by

$$t_i = t_{i-1} + \Delta t_i, \tag{7}$$

$$\Delta t_i = A\Delta t_{i-1}, \tag{8}$$

where Δt_i is the time width of the ith time bin and A is a constant, which is estimated using the first time bin t_1 and last time bin of the analysis $t_{\rm end}$. In this paper, we use $\Delta t_1 = 0.5$ and $t_{\rm end} = 100$ s, respectively, and the number of bins $N = 20$, such that $A \approx 1.206$. To calculate the χ^2 in Equation (5) the central value of the time bin $(t_i - 0.5\Delta t_i)$ is used as shown in Figure 2.

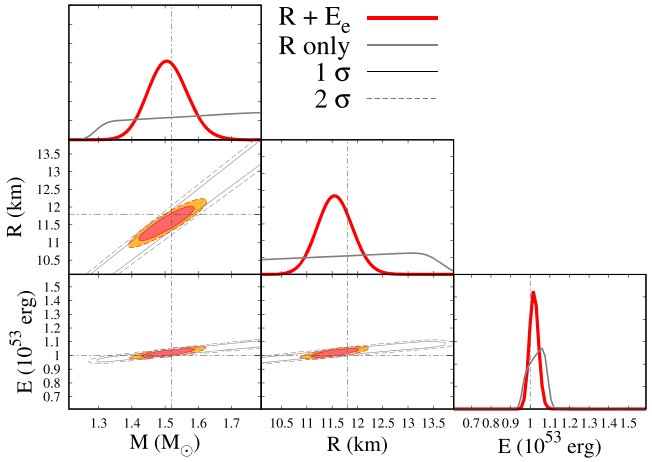

Figure 3. Probability density function (PDF) determined by Equation (6) for the simulation in Figure 2. Contours with solid and dashed lines correspond to $\mathcal{P}/\mathcal{P}_{\rm max} = 1/e$ (0.368, corresponding to 1σ) and $1/e^2$ (0.135, 2σ), respectively, where $\mathcal{P}_{\rm max}$ is the maximum value of the PDF. Colored lines give results using both the event rate and average energy of the positrons, while gray lines give those from the fit with the event rate alone.

Error bars in the figure indicate the Poisson statistical error on the event rate and the standard deviation of energies in each bin for the average energy plot. Since the error bars of the energies are mostly determined by the spectrum of positrons, which originates from the neutrino spectrum, the error bars become smaller at the late phase than at the early phase because the average energy becomes smaller. Two solid lines (red and gray) show the time evolution of the event rate and average energy using the best-fit parameters. The gray line is calculated by the event rate alone, but the red line is calculated by both the event rate and the average energy data. For the latter the χ^2 is estimated by the simple sum of the contributions at each time step from the event rate and average energy.

We next estimate the uncertainties of the model parameters with the PDF of Equation (6). Figure 3 shows the distribution of $\mathcal{P}$. In this figure contours with solid and dashed lines correspond to $\mathcal{P}/\mathcal{P}_{\rm max} = 1/e$ (0.368, corresponding to 1σ) and $1/e^2$ (0.135, 2σ), respectively, where $\mathcal{P}_{\rm max}$ is the maximum value of $\mathcal{P}$. Colored lines give results with both $\mathcal{R}$ and E_{e^+}, but gray lines give those with $\mathcal{R}$ alone. Due to the parameter degeneracy, the allowed regions in M and R are rather large and elongated for the case with $\mathcal{R}$ alone. However, $E_{\rm tot}$ can be estimated accurately even using only $\mathcal{R}$. We can draw the same conclusion from the marginalized PDFs shown in the top panel of each column. Note that the uncertainties shown here are for a single realization. Since the observed data are subject to fluctuations due to Poisson statistics, it is necessary to perform Monte Carlo calculations for multiple realizations in order to evaluate the expected parameter sensitivity (expected error) in anticipation of an actual observation.

4. Parameter Sensitivity

The expected parameter sensitivity is evaluated using 100 realizations of the model above. Figure 4 shows the resulting PDFs of $M_{\rm PNS}$, $R_{\rm PNS}$, and $E_{\rm tot}$, respectively, for each realization. The bold lines indicate their averages. Each Monte Carlo calculation produces various best-fit values according to Poisson statistics, but the average line shows that the input values are the most plausible and that values far from the input

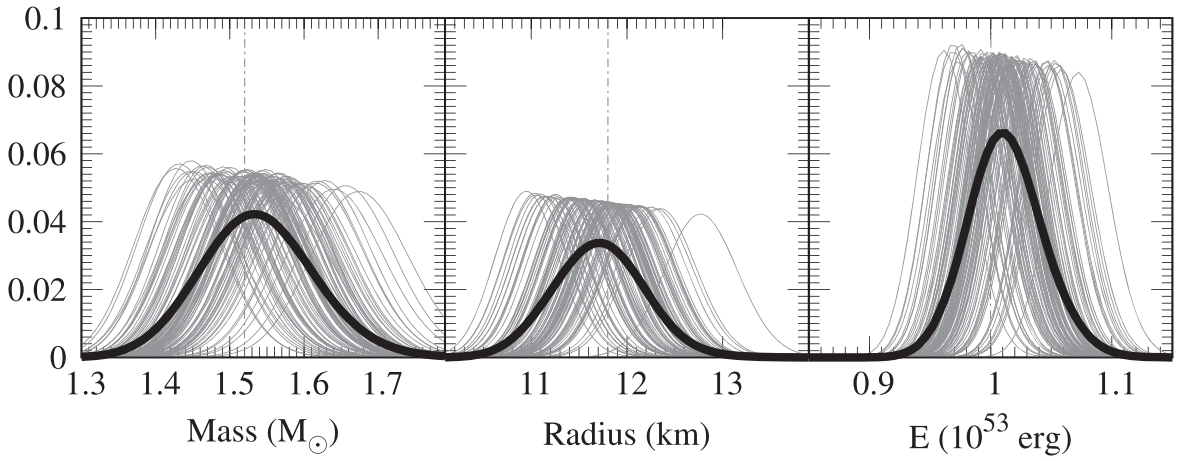

Figure 4. PNS parameter PDFs, $M_{\rm PNS}$, $R_{\rm PNS}$, and $E_{\rm tot}$, respectively, for 100 realizations.

result in a predominant drop in the probability density. Note that the average PDF taken over 1000 realizations shows almost the same distribution. Our estimate of the expected parameter sensitivity uses the median value of the average PDF as the central value and the uncertainties 68% and 95% given by the parameter range that represent those probability contents (taken about the median). The results are summarized in Table 1.

Figure 5 shows a histogram of the distribution of best-fit values for 100,000 realizations, with the average PDF shown as a red line. From this figure, we can see that the average PDF of 100 realizations is roughly equivalent to the best-fit fluctuations of the larger statistics. The slight deviation of the maximum of the best-fit value distribution from the input suggests that the fitting contains some bias. Since the goal of this paper is to demonstrate a simple model analyzed in a simple manner; we will not go into depth here.

Here we have only demonstrated the expected sensitivity for a specific choice of $M_{\rm PNS}$, $R_{\rm PNS}$, and $E_{\rm tot}$. Calculations performed for $1.2M_\odot < M_{\rm PNS} < 1.8M_\odot$ and 10 km $< R_{\rm PNS} <$ 14 km,[12] however, yield similar parameter uncertainties. This can be understood from the limited dependence of $M_{\rm PNS}$ and $R_{\rm PNS}$ on the total number of events, as given by Equation (3).

Table 1
Expected Values and Statistical Errors

	Median	68%	95%
$M_{\rm PNS}$ ($M_\odot$)	1.532	$^{+0.079}_{-0.075}$	$^{+0.163}_{-0.147}$
$R_{\rm PNS}$ (km)	11.69	$^{+0.48}_{-0.48}$	$^{+0.98}_{-0.93}$
$E_{\rm tot}$ (10^{53} erg)	1.009	$^{+0.032}_{-0.030}$	$^{+0.066}_{-0.059}$

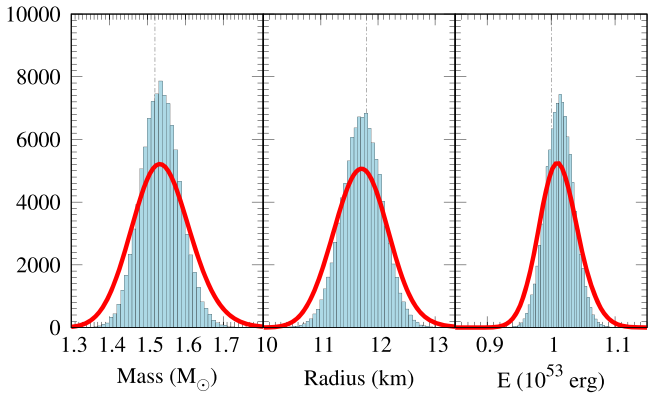

Figure 5. Comparison of the distributions of the best-fit values of the PNS parameters (histogram) and their average PDFs (solid line). The histogram is drawn with 100,000 realizations and the solid lines with 100.

5. Summary

In this paper, we performed Monte Carlo sampling calculations of neutrino events observed in Super-Kamiokande from a Galactic SN explosion. The analytical solution from Suwa et al. (2021) was used as the theoretical template for the event rate and the event spectrum of the inverse beta decay interactions. Model parameter estimation was performed on these mock sampling data using a simple least-squares method. The results show that the mass, radius, and total energy can be determined with an accuracy of $\sim 0.1\ M_\odot$, $\sim$1 km, and $\sim 10^{51}$ erg, respectively, for a Galactic SN at 8 kpc.

We have focused specifically on the late neutrino emission from SNe, since it depends on only a few physical quantities, such as the mass and radius of the neutron star. Importantly, both of these are reflected in the neutrino signal. However, since the present method does not include the early-phase emission, the total event energy cannot be in this context (see, e.g., Nagakura & Vartanyan 2022, for early emission). The next step is to establish a methodology to approach the physical quantities of both the late and early neutrino emission. This requires the development of a method to analyze numerical calculations of the complete neutrino emission over all time domains. The methodology presented in this paper is the first step toward this goal.

This work is supported by Grant-in-Aid for Scientific Research (20H00174, 20H01904, 20K03973) and Grant-in-Aid for Scientific Research on Innovative Areas (17H06357, 17H06365, 18H05437, 19H05811, 20H04747, 22H04571) from the Ministry of Education, Culture, Sports, Science and Technology (MEXT), Japan. This work was partly supported by MEXT as "Program for Promoting Researches on the Supercomputer Fugaku" (Toward a unified view of the universe: from large scale structures to planets). This work was partially carried out by the joint research program of the

[12] $E_{\rm tot}$ is not changed since it is strongly related to the early phase.

Institute for Cosmic Ray Research (ICRR), The University of Tokyo.

Appendix
Energy Distribution of Positrons

We employ the Fermi–Dirac distribution for the neutrinos and the resultant positron energy spectrum is given as

$$f(E) \propto \frac{E^4}{1 + \exp(E/k_{\rm B}T_\nu)}, \tag{A1}$$

where $k_{\rm B}$ is the Boltzmann constant and T_ν is the temperature characterizing the intrinsic neutrino spectrum. Note that T_ν evolves with time as the PNS cools. This spectrum is derived from the thermal neutrino spectrum ($\propto E^2/(1 + \exp(E/k_{\rm B}T))$) and using the inverse beta cross section ($\propto E^2$). It relates to Equation (4) as $E_{e^+} = \int Ef(E)dE \Big/ \int f(E)dE$ (see Suwa et al. 2021, for details).

ORCID iDs

Yudai Suwa https://orcid.org/0000-0002-7443-2215
Akira Harada https://orcid.org/0000-0003-1409-0695
Yusuke Koshio https://orcid.org/0000-0003-0437-8505
Masamitsu Mori https://orcid.org/0000-0002-0827-9152
Ken'ichiro Nakazato https://orcid.org/0000-0001-6330-1685
Kohsuke Sumiyoshi https://orcid.org/0000-0002-9224-9449

References

Adams, S. M., Kochanek, C. S., Beacom, J. F., Vagins, M. R., & Stanek, K. Z. 2013, ApJ, 778, 164
Bollig, R., Yadav, N., Kresse, D., et al. 2021, ApJ, 915, 28
Burrows, A. 1988, ApJ, 334, 891
Burrows, A., & Vartanyan, D. 2021, Natur, 589, 29
Fischer, T., Hempel, M., Sagert, I., Suwa, Y., & Schaffner-Bielich, J. 2014, EPJA, 50, 46
Fischer, T., Whitehouse, S. C., Mezzacappa, A., Thielemann, F. K., & Liebendörfer, M. 2010, A&A, 517, A80
Horiuchi, S., & Kneller, J. P. 2018, JPhG, 45, 043002
Hüdepohl, L., Müller, B., Janka, H. T., Marek, A., & Raffelt, G. G. 2010, PhRvL, 104, 251101
Li, S. W., Roberts, L. F., & Beacom, J. F. 2021, PhRvD, 103, 023016
Mirizzi, A., Tamborra, I., Janka, H. T., et al. 2016, NCimR, 39, 1
Mori, M. 2021, PhD thesis, Kyoto Univ.
Mori, M., Suwa, Y., Nakazato, K., et al. 2021, PTEP, 2021, 023E01,
Nagakura, H., Burrows, A., & Vartanyan, D. 2021, MNRAS, 506, 1462
Nagakura, H., & Vartanyan, D. 2022, MNRAS, 512, 2806
Nakamura, K., Horiuchi, S., Tanaka, M., et al. 2016, MNRAS, 461, 3296
Nakamura, K., Takiwaki, T., & Kotake, K. 2019, PASJ, 71, 98
Nakazato, K., Nakanishi, F., Harada, M., et al. 2022, ApJ, 925, 98
Nakazato, K., Sumiyoshi, K., Suzuki, H., et al. 2013, ApJS, 205, 2
Pascal, A., Novak, J., & Oertel, M. 2022, MNRAS, 511, 356
Roberts, L. F., Shen, G., Cirigliano, V., et al. 2012, PhRvL, 108, 061103
Sato, K., & Suzuki, H. 1987, PhLB, 196, 267
Scholberg, K. 2012, ARNPS, 62, 81
Strumia, A., & Vissani, F. 2003, PhLB, 564, 42
Super-Kamiokande Collaboration, Mori, M., et al. 2022, arXiv:2206.01380
Suwa, Y. 2014, PASJ, 66, L1
Suwa, Y., Harada, A., Nakazato, K., & Sumiyoshi, K. 2021, PTEP, 2021, 013E01
Suwa, Y., Sumiyoshi, K., Nakazato, K., et al. 2019, ApJ, 881, 139
Vartanyan, D., Burrows, A., & Radice, D. 2019, MNRAS, 489, 2227
Vogel, P., & Beacom, J. F. 1999, PhRvD, 60, 053003
Warren, M. L., Couch, S. M., O'Connor, E. P., & Morozova, V. 2020, ApJ, 898, 139